being associated with the $CrPh_5^{2-}$ moiety. In this compound the Cr–C distances average 2.09 Å whereas in 4 they average an even shorter 2.06 Å. These bonds are a good deal shorter than those seen in 2 whose Cr–C distances average 2.24 Å. Similar arguments to those employed for the vanadium complex can be invoked to account for the long bonds. Obviously, the higher coordination in 2 compared to that in 3 and the greater negative charge of the $CrPh_6^{3-}$ moiety compared to those of 3 and the neutral 4 are factors in the lengthening of the bonds. In addition, all the Cr–C bonds in 2 are bridging whereas in 4 all the bonds are terminal. In comparison to the vanadium complex 1, the Cr–C bonds in 2 are shorter because of the higher metal oxidation state and that Cr, being farther to the right in the periodic table, is smaller than V. The octahedral coordination is again favored by the d^3 electron configuration. The Li–C bonds are very similar to those seen in 1. Another interesting feature of 2 is the asymmetric disposition of the Li^+ ions relative to the $CrPh_6^{3-}$ moiety. A more symmetric distribution could have been achieved if the Li bridged edges of the C_6 octahedron. Indeed, this is the case in the complex $Li_3CrMe_6 \cdot 6$-(0.5dioxane) (5) whose Cr–C distances are also exceedingly long at 2.3 Å as are the Cr–Li vectors at 2.7 Å. It could be argued that since CH_3^- is expected to be a better σ-donor than Ph^-, there is greater negative charge buildup in 5 and longer Cr–C bonds. In that case shorter Cr–Li contacts than those seen in 2 would be expected. However, longer distances, 2.7 vs 2.66 Å, are observed. This is probably a result of the different coordination spheres surrounding the Li^+ ions in the complexes. In 5, each Li^+ is coordinated to two strongly coordinating dioxanes, and as a result, the Li^+ ions are disposed to interact with two rather than three carbons. This results in the Li^+ ions bridging C_6 octahedron edges in 5 rather than their faces which is what is observed in 2.

In summary our results show that it is possible to fairly readily crystallize polyphenylated/Li^+ salts of some early transition metals. Presumably, similar crystallographic studies can be carried out on species of the group 4 transition metals as well as heavier members of group 6. Studies on these and related species are continuing.

Acknowledgment. We thank the donors Petroleum Research Fund, administered by the American Chemical Society, for financial support.

Registry No. 1, 113858-41-6; 2, 113858-42-7; VCl_3, 7718-98-1; $CrCl_2$, 10049-05-5; PhLi, 591-51-5.

Supplementary Material Available: Tables of bond distances and angles, anisotropic thermal parameters, and hydrogen coordinates (18 pages); listings of structural factors (87 pages). Ordering information is given on any current masthead page.

How Do μ_2-Bridging Ligands Affect Metal–Metal Bonds in a Triosmium or Triruthenium Framework

Catherine E. Housecroft* and Steven M. Owen

University Chemical Laboratory, Lensfield Road, Cambridge CB2 1EW, U.K.

Received November 23, 1987

Fenske–Hall quantum chemical calculations have been performed on model complexes of general formula $HRu_3(CO)_{10}X$ (X = Cl, SH, and PH_2) in order to investigate the pattern in bonding of the μ_2-bridging groups to the metal framework in compounds $HM_3(CO)_{10}X$ (M = Ru and X = PHPh or SEt; M = Os and X = H, Cl, PHPh, SEt, $SCHPh_2$, or SC(H)=N-*p*-C_6H_4-F). It is shown that in the model compound $HRu_3(CO)_{10}SH$, the strengthening effect of the μ-SH group on the bridged metal–metal bond outweighs the weakening caused by the μ-H atom. The metal to main-group atom bridge bonding, rather than the direct metal–metal overlap, is responsible for the observed shortening of the bridged metal–metal bond, but the gross changes in metal–metal bonding caused by the bridging groups within the M(μ-H)(μ-X)M system are finely tuned by direct metal–metal overlap. Periodic trends as the group X varies in the model compound $HRu_3(CO)_{10}X$ are discussed. Along the series where X = PH_2, SH, or Cl, we show that the observed trend in bridged metal–metal bond lengths may be primarily attributed to a weakening of the interaction between the trimetal framework and the tangential orbital which is common to all three bridging groups. Changes in hybridization at the bridgehead atom, caused by the decreasing number of attached hydrogen atoms along the series, result in further perturbation of the trimetal to main-group interfragment bonding.

There is now characterized a wide variety of metal complexes of the general formula $HM_3(CO)_{10}X$ (M = Ru or Os), where X (X is group containing a second-row, group 15, 16, or 17 atom) and H are μ_2-ligands bridging the same metal–metal bond.[1-6] Other related complexes with first-row bridge groups have also been characterized.[7-15] It is well-known from the work of, for example, Churchill

Chart I

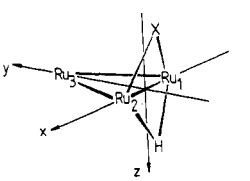

(1) Churchill, M. R.; Lashewycz, R. A. *Inorg. Chem.* **1979**, *18*, 1926.
(2) Iwasaki, F.; Mays, M. J.; Raithby, P. R.; Taylor, P. L.; Wheatley, P. J. *J. Organomet. Chem.* **1981**, *213*, 185.
(3) Mays, M. J.; Pavelcik, F.; Raithby, P. R.; Taylor, P. L.; Wheatley, P. J. *Acta Crystallogr., Sect. B: Struct. Crystallogr. Cryst. Chem.* **1981**, *37B*, 2228.
(4) Adams, R. D.; Dawoodi, Z. *J. Am. Chem. Soc.* **1981**, *103*, 6510.
(5) Holden, H. D.; Johnson, B. F. G.; Lewis, J.; Raithby, P. R.; Uden, G. *Acta Crystallogr., Sect. B: Struct. Crystallogr. Cryst. Chem.* **1981**, *39B*, 1200.
(6) Churchill, M. R.; Ziller, J. W.; Keister, J. B. *J. Organomet. Chem.* **1985**, *297*, 93.
(7) Podberezskaya, N. V.; Maksakov, V. A.; Kedrova, L. K.; Korniets, E. D.; Gubin, S. P. *Koord. Khim.* **1984**, *10*, 919.
(8) D'Ornelas, L. D.; Choplin, A.; Basset, J. J.; Hsu, L.-Y.; Shore, S. G. *Nouv. J. Chim.* **1985**, *9*, 155.

0276-7333/88/2307-1385$01.50/0

Table I. M-M Bond Distances in $M_3(CO)_{12}$ and $HM_3(CO)_{10}X$

M	X	bridged/Å	unbridged/Å	ref
		$HM_3(CO)_{10}X$		
Os	Cl	2.846 (1)	2.829 (1), 2.836 (1)	1
Ru	>PHPh	2.903 (1)	2.853 (1), 2.848 (1)	2
Os	>PHPh	2.917 (4)	2.867 (4), 2.895 (4)	3
Os	>S-C(H)=N-*p*-C_6H_4-F	2.870 (1)	2.860 (1), 2.868 (1)	4
Os	>$SCHPh_2$	2.867 (2)	2.846 (2), 2.862 (2)	5
Ru	>SEt	2.843 (1)	2.831 (2), 2.824 (1)	6
		$M_3(CO)_{12}$		
Ru			2.854 (4)	17a
Os			2.877 (3)	17b

et al.[1,16] that a single hydrogen atom bridging a metal–metal vector in an Ru_3 or Os_3 triangle causes an increase in the M–M distance compared to the respective bond length in the parent compound $M_3(CO)_{12}$.[17] This increase is generally greater than 0.1 Å. However, in complexes of the type $HM_3(CO)_{10}X$ (M = Ru or Os) shown in Chart I, the bridged M–M bond may be shorter than, approximately equal to, or longer than the corresponding M–M bond in the parent trimetal binary carbonyl compound.[12] The observed trends are illustrated in Table I. The trends in some of the osmium clusters have been related to the covalent radius of the bridgehead atom;[14] for example, in $HOs_3(CO)_{10}X$ with the bridgehead atom being a second-row element, the bridged Os–Os bond length decreases along the series X = PR_2 > SR > Cl, i.e. as the covalent radius of the bridgehead atom decreases. However, this explanation leaves some anomalies, although it may be argued that steric constraints imposed by the bridging ligand as a whole are, in some cases, significant and may override trends set by the bridgehead atom itself.

We have undertaken an examination of the electronic properties of the $[Ru_3(CO)_{10}]^{2-}$ fragment and present here the interactions of this fragment with μ_2-bridging groups H and X (X = Cl, SH, PH_2). The consequences of these interactions are discussed with particular note being paid to the effects upon the metal–metal bonding of the Ru(μ-X)(μ-H)Ru bond. Previous calculations by Hall et al. have shown these to be only weak Os–Os bonding between the bridged atoms of $HOs_3(CO)_{10}X$ (X = Cl, Br, I).[18]

Experimental Section

Fenske–Hall[19] calculatons were carried out on the compounds $HRu_3(CO)_{10}X$ where X = PH_2, SH,[20] or Cl. These complexes act as models for experimentally characterized compounds of general formula $HM_3(CO)_{10}X$ (M = Ru and X = PHPh or SEt; M = Os and X = Cl, PHPh, SEt, $SCHPh_2$, or SC(H)=N-*p*-C_6H_4-F). Two calculations were carried out for each compound. The first used a geometry for the triruthenium fragment based on the geometry of the experimental parent compound; bond distances used are summarized in Table IIa. The second calculation used a fixed $[HRu_3(CO)_{10}]^-$ fragment geometry for each compound (Table IIb). Comparison of the results of the two calculations tested whether changes in Mulliken overlap populations were actually due to changing the bridging ligand X and were not simply artifacts due to changes in the Ru–Ru bond lengths. In all cases, the $HRu_3(CO)_{10}X$ molecule was idealized to C_s symmetry with the mirror plane passing through H, X, and Ru(3) (Chart I). All carbonyl ligands were terminal; C–O bonds were set at 1.13 Å, and Ru–CO bonds were 1.90 Å. Atomic numbering and the axis system for the calculations are shown in Chart I; in $HRu_3(CO)_{10}X$, atoms Ru(1) and Ru(2) are symmetry-related.

Table II. Bond Distances Used in Fenske–Hall Calculations

a. Geometries Based on Experimentally Determined Structures of Parent Compounds

model compd	bond type	length/Å	ref
$HRu_3(CO)_{10}Cl$[a]	Ru–Ru(bridged)	2.846	1
	Ru–Ru(unbridged)	2.832	
	Ru–Cl	2.456	
	Ru–H	1.850	
$HRu_3(CO)_{10}SH$[b]	Ru–Ru(bridged)	2.840	6
	Ru–Ru(unbridged)	2.827	
	Ru–S	2.389	
	S–H	1.340	
	Ru–H	1.761	
$HRu_3(CO)_{10}PH_2$[b]	Ru–Ru(bridged)	2.900	2
	Ru–Ru(unbridged)	2.849	
	Ru–P	2.337	
	P–H	1.410	
	Ru–H	1.861	

b. Fixed Geometry for $[HRu_3(CO)_{10}]^-$ Fragment[c]

bond type	bond length/Å
Ru–Ru(unbridged)	2.854
Ru–Ru(bridged)	2.854
Ru–μ-H	1.800

[a] Structural parameters are based on those of the related osmium compound (Table I). [b] Structural parameters are based on those of the related ruthenium compound (Table I). [c] Ru–X bond lengths are as given in Table IIa.

The Fenske–Hall calculations employed single-ζ Slater functions for the 1s and 2s functions of C, O, P, and S. The exponents were obtained by curve fitting the double-ζ functions of Clementi[21] while maintaining orthogonal functions; the double-ζ functions were used directly for the 2p orbitals. An exponent of 1.16 was used for hydrogen. The Ru functions,[22] chosen for the +1 oxidation state, were augmented by 5s and 5p functions with exponents of 2.20.

Results and Discussion

The fragment $[Ru_3(CO)_{10}]^{2-}$ is common to all the compounds of type $HM_3(CO)_{10}X$ discussed in this paper. The two axial and two equatorial carbonyl ligands on Ru(3) (Chart I) reflect the same ligand positions found in $Ru_3(CO)_{12}$. The three carbonyls on each of atoms Ru(1) and Ru(2) in $[Ru_3(CO)_{10}]^{2-}$ are generated from those in $Ru_3(CO)_{12}$ by the removal of one ligand (either axial or equatorial) followed by a reorientation of the three remaining ligands. The consequences of such a rearrangement on the frontier orbitals of the metal carbonyl fragment have previously been assessed in connection with the

(9) Banford, J.; Mays, M. J.; Raithby, P. R. *J. Chem. Soc., Dalton Trans.* **1985**, 1355.
(10) Churchill, M. R.; DeBoer, B. G.; Rotella, F. J. *Inorg. Chem.* **1976**, *15*, 1843.
(11) Boag, N. M.; Kampe, C. E.; Lin, Y. C.; Kaesz, H. D. *Inorg. Chem.* **1982**, *21*, 1707.
(12) Churchill, M. R.; Wasserman, H. J. *Inorg. Chem.* **1981**, *20*, 1580.
(13) Dawoodi, Z.; Mays, M. J.; Hendrick, K. *J. Chem. Soc., Dalton Trans.* **1984**, 433.
(14) Churchill, M. R.; Wasserman, H. J. *Inorg. Chem.* **1981**, *20*, 2905.
(15) Burgess, K.; Johnson, B. F. G.; Lewis, J.; Raithby, P. R. *J. Chem. Soc., Dalton Trans.* **1982**, 263.
(16) Churchill, M. R. *Adv. Chem. Ser.* **1978**, *No. 167*, 36–60.
(17) (a) Churchill, M. R.; Hollander, F. J.; Hutchison, J. P. *Inorg. Chem.* **1977**, *16*, 2655. (b) Churchill, M. R.; DeBoer, B. G. *Inorg. Chem.* **1977**, *16*, 878.
(18) Chesky, P. T.; Hall, M. B. *Inorg. Chem.* **1983**, *22*, 3327.
(19) Hall, M. B.; Fenske, R. F. *Inorg. Chem.* **1972**, *11*, 768.
(20) The validy of PH_3 as a model for PPh_3 in Fenske–Hall calculations has been tested: Kostic, N. M.; Fenske, R. F. *Organometallics* **1982**, *1*, 489. Here we use PH_2 and SH to model PHPh and SR′, respectively.
(21) Clementi, E. *J. Chem. Phys.* **1964**, *40*, 1944.
(22) Richardson, J. W.; Blackman, M. J.; Ranochak, J. F. *J. Chem. Phys.* **1973**, *58*, 3010.
(23) Kostic, N. M.; Fenske, R. F. *Organometallics* **1982**, *1*, 974.

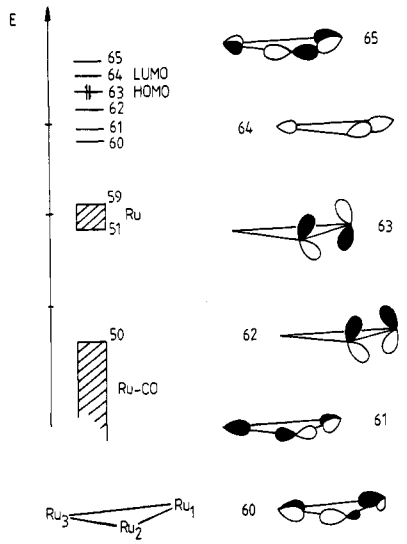

Figure 1. Frontier molecular orbitals of the fragment $[Ru_3(CO)_{10}]^{2-}$. The symmetry properties of the orbitals do not change as the metal–metal bond lengths are altered in the series of compounds $HRu_3(CO)_{10}X$ (X = Cl, PH_2, SH).

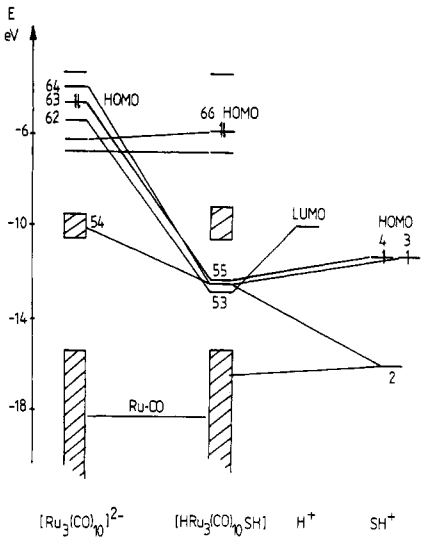

Figure 2. An orbital correlation diagram for the formation of $HRu_3(CO)_{10}SH$ from $[Ru_3(CO)_{10}]^{2-}$, H^+, and SH^+ fragments. The fragment MO energies are taken from the Fock matrix of the complex.[23]

binding of acetylene ligands to the $Ru_3(CO)_8$ fragment.[24] The carbonyl rearrangement is necessary if the metal framework is to accommodate two ligands, one on each side of the M_3 triangle. The frontier orbitals of the idealized $[Ru_3(CO)_{10}]^{2-}$ fragment are schematically represented in Figure 1. The second highest occupied molecular orbital, MO 62, is Ru(1)–Ru(2) bonding, and 70% of the total orbital character is located on these two metal atoms. The HOMO, MO 63, is Ru(1)–Ru(2) antibonding, and, again, 70% orbital character is centered on Ru(1) and Ru(2). The LUMO, MO 64, is bonding around the metal triangle; 59% of the orbital's character is located on the three metal atoms, a total of 53% being associated with Ru(1) and Ru(2).

Interaction of $[Ru_3(CO)_{10}]^{2-}$ with H^+. Since the bridging hydrogen atom in $HRu_3(CO)_{10}X$ is equidistant from atoms Ru(1) and Ru(2), the 1s orbital of the hydrogen atom is compatible in terms of symmetry with only MO's 61, 62, and 64 of the metal fragment (Figure 1). With the lobes of the orbital pointing above and below the metal triangle, MO 62 is ideally suited to interact efficiently with the 1s AO of H^+. This is indeed the primary Ru(1)–μ-H–Ru(2) interaction, and significant depopulation of MO 62 results, causing the metal–metal bond to weaken and, thus, lengthen as observed experimentally in related systems.[10,16]

Interaction of $[Ru_3(CO)_{10}]^{2-}$ with H^+ and SH^+. Each of the ligands X discussed here possesses tangential (parallel to the M–M vector) and radial (perpendicular to the M–M vector) atomic or molecular frontier orbitals. The hybridization of the atomic orbitals on the bridgehead atom is obviously a function of the number of hydrogen atoms attached, e.g. along the series Cl, SH, PH_2. The consequences of altering the hybridization is discussed later in this paper. First, however, we exemplify the interaction of the bridging ligands with the metal framework by looking at the orbital interactions of H^+ and SH^+ with $[Ru_3(CO)_{10}]^{2-}$. A correlation diagram for the interaction of the frontier orbitals of the three fragments to form $HRu_3(CO)_{10}SH$ is given in Figure 2. The MO's of the complex are categorized as follows. There is a low-lying set of MO's involved mainly in Ru–CO bonding: included in this set are low-energy orbitals of the SH ligand which

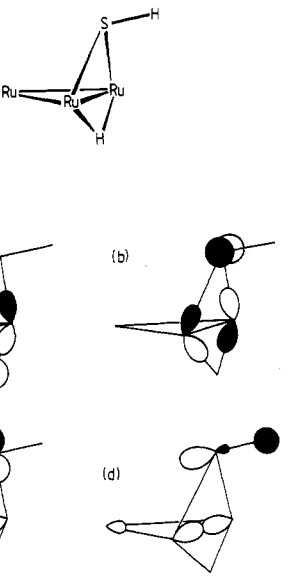

Figure 3. Fragment–fragment orbital interactions in $HRu_3(CO)_{10}SH$: (a) MO 62 of $[Ru_3(CO)_{10}]^{2-}$ with 1s orbital of H^+; (b) MO 63 of $[Ru_3(CO)_{10}]^{2-}$ with MO 4 (tangential) of SH^+; (c) MO 64 of $[Ru_3(CO)_{10}]^{2-}$ with MO 3 (radial) of SH^+; (d) MO 64 of $[Ru_3(CO)_{10}]^{2-}$ with MO 2 (derived from radial orbitals) of SH^+.

are not involved in binding the ligand to the metal framework. MO's 56–64 contain mostly metal d character, the so-called "pseudo t_{2g} set" of orbitals.[25,26] MO 66 (HOMO) and MO 65 are triruthenium-based orbitals which are derived directly from the $[Ru_3(CO)_{10}]^{2-}$ fragment MO's 60 and 61. The metal–μ-H and metal–μ-SH bonding character is localized in four orbitals in the complex, viz. MO's 51 and 53–55. As in $[HRu_3(CO)_{10}]^-$, the 1s orbital of the proton interacts with MO 62 of the $[Ru_3(CO)_{10}]^{2-}$ fragment. MO 2 (radial) of the SH^+ fragment interacts with metal fragment MO 64; the interfragment Mulliken overlap populations indicate that involvement of MO 2 is not as significant as that of the second radial orbital of SH^+, MO 3. MO's 3 and 4 (singly occupied degenerate

(24) Housecroft, C. E.; Owen, S. M. *J. Organomet. Chem.* **1988**, *339*, 139.

(25) Mingos, D. M. P.; Forsyth, M. I. *J. Chem. Soc., Dalton Trans.* **1977**, 610.

(26) Schilling, B. E. R.; and R. Hoffmann *J. Am. Chem. Soc.* **1979**, *101*, 3456.

Table III. Fragment–Fragment Mulliken Overlap Populations for the Formation of $HRu_3(CO)_{10}SH$ from $[Ru_3(CO)_{10}]^{2-}$, SH^+, and H^+

MO in $[Ru_3(CO)_{10}]^{2-}$ fragment	MO in SH^+ fragment			H^+ 1s AO
	2	3 (HOMO)	4 (HOMO)	
62	0.013	0.013		0.260
63 (HOMO)			0.159	
64 (LUMO)	0.051	0.114		

Table IV. Mulliken Populations of Frontier Orbitals of the Fragments $[Ru_3(CO)_{10}]^{2-}$, $[X]^+$, and H^+ after the Formation of $HRu_3(CO)_{10}X$

fragment MO of $[Ru_3(CO)_{10}]^{2-}$	Mulliken pop. of fragment MO's in $[Ru_3(CO)_{10}]^{2-}$ as a function of X^+		
	PH_2^+	SH^+	Cl^+
62	0.73	0.73	0.68
63 (HOMO)	0.56	0.41	0.30
64 (LUMO)	0.41	0.35	0.34
fragment MO[a] of $[X]^+$	Mulliken pop. of fragment MO's in $[X]^+$ as a function of X^+		
	PH_2^+	SH^+	Cl^+
2	2.00	1.85	1.95
3 (radial)	1.51	1.72	1.72
4 (tangential)	1.37	1.55	1.67
	Mulliken pop. of H^+ AO as a function of X^+		
	PH_2^+	SH^+	Cl^+
H^+ AO	1.34	1.31	1.34

[a] For Cl^+, MO's 2–4 are triply degenerate HOMO; for SH^+, MO's 3 and 4 are doubly degenerate HOMO; for PH_2^+, MO 4 is the HOMO.

HOMO's) of the SH^+ unit interact with MO's 64 and 63, respectively, of the $[Ru_3(CO)_{10}]^{2-}$ fragment. Note that the respective directionalities of the SH^+ frontier orbitals 3 and 4 (but to a lesser extent those of MO 2) are beautifully compatible with the in-plane nature of metal fragment MO 64 and out-of-plane nature of MO 63 (Figure 3). Again, we draw attention to the fact that the orientation of the carbonyl ligands attached to atoms Ru(1) and Ru(2) is intimately responsible, from the metals' point of view, for this interfragment orbital compatibility. Table III shows the Mulliken overlap populations between fragments for the frontier orbital interactions.

The middle column in Table IV lists the occupancies, after complex formation, of those $[Ru_3(CO)_{10}]^{2-}$, SH^+, and H^+ fragment orbitals which are involved in interfragment bonding. The major changes in orbital occupancies arise from interactions involving MO's 62–64 of the $[Ru_3(CO)_{10}]^{2-}$ fragment. The numbers tabulated reiterate the correlations made in Figure 2; electrons lost from MO 62 of the metal fragment are balanced by the gain in the hydrogen 1s orbital, while the fractional occupancies of MO's 63 and 64 of $[Ru_3(CO)_{10}]^{2-}$ correspond to a net transfer of charge to the radial (MO 3) and tangential (MO 4) orbitals of SH^+. In terms of affecting the triruthenium framework, interaction with H^+ withdraws electron density from MO 62 and weakens the Ru(1)–Ru(2) bond. On the other hand, interaction with SH^+ depopulates the initial HOMO (MO 63) and populates the LUMO of the trimetal fragment causing strengthening of Ru(1)–Ru(2). It is important to realize that MO's 62 and 63 of the $[Ru_3(CO)_{10}]^{2-}$ fragment have the same parentage and are π-bonding and antibonding analogues of one another; both MO's possess the same percentage of Ru(1) and Ru(2) character. Therefore, we are justified in making a direct comparison between the charge lost by MO's 62 and 63 in terms of

Table V

bond	PH_2	SH	Cl
(a) Interatomic Mulliken Overlap Populations in Complexes $[Ru_3(CO)_{10}X]^-$			
Ru(1)–Ru(2)	+0.097	+0.123	+0.132
Ru(1)–$X_{bridgehead\text{-}atom}$[a]	+0.213	+0.151	+0.109
(b) Interatomic Mulliken Overlap Populations in Complexes $[HRu_3(CO)_{10}X]$			
Ru(1)–Ru(2)	+0.014	+0.025	+0.038
Ru(1)–$X_{bridgehead\ atom}$[a]	+0.213	+0.160	+0.120
Ru(1)–H[a]	+0.131	+0.150	+0.133

[a] Ru(1)–$X_{bridgehead\text{-}atom}$ = Ru(2)–$X_{bridgehead\text{-}atom}$; Ru(1)–H = Ru(2)–H.

metal–metal bond weakening and strengthening, respectively. Thus, the results in Table IV suggest that the strengthening of Ru(1)–Ru(2) caused when the SH^+ group interacts with the metal triangle outweighs the weakening due to the presence of the bridging hydrogen atom. This point is investigated further by considering the effect on the Ru(1)–Ru(2) bond of protonating the $[Ru_3(CO)_{10}SH]^-$ anion.

Protonation of $[Ru_3(CO)_{10}SH]^-$. The formation of $[Ru_3(CO)_{10}SH]^-$ from the fragments $[Ru_3(CO)_{10}]^{2-}$ and SH^+ is accompanied by the stabilization of metal fragment MO's 63 and 64, as expected from Figure 2. MO 62 of $[Ru_3(CO)_{10}]^{2-}$ becomes the HOMO of $[Ru_3(CO)_{10}SH]^-$ and remains essentially unperturbed. A comparison of the Mulliken populations of the $[Ru_3(CO)_{10}]^{2-}$ fragment orbitals in both $[Ru_3(CO)_{10}SH]^-$ and $HRu_3(CO)_{10}SH$ reflects the fact that the SH^+ group has interacted with $[Ru_3(CO)_{10}]^{2-}$ in much the same way in both complexes; the fractional occupancies of the fragment $[Ru_3(CO)_{10}]^{2-}$ MO's 63 and 64 are 0.38 and 0.53 electron, respectively, in $[Ru_3(CO)_{10}SH]^-$ compared to 0.41 and 0.35 electron in $HRu_3(CO)_{10}SH$. As expected, on protonating $[Ru_3(CO)_{10}SH]^-$, the HOMO is stabilized to give the localized Ru(1)–μ-H–Ru(2) bonding orbital of the neutral complex illustrated in Figure 2.

Consider, now, the direct metal–metal bonding in $[Ru_3(CO)_{10}SH]^-$ and $HRu_3(CO)_{10}SH$. In the fragment $[Ru_3(CO)_{10}]^{2-}$, the total Ru(1)–Ru(2) overlap is +0.039. This increases to +0.123 in $[Ru_3(CO)_{10}SH]^-$, a value which is comparable to an overlap of +0.111 between adjacent ruthenium atoms in $Ru_3(CO)_{12}$. Protonation of $[Ru_3(CO)_{10}SH]^-$ results in a decrease in the Ru(1)–Ru(2) overlap to +0.025. However, it is dangerous to conclude that this dramatic decrease in metal–metal overlap population necessarily leads to metal–metal bond *lengthening*, since it has been shown previously that metal–metal bond *shortening* may be produced indirectly by a "clamping" effect of the bridging ligands.[24,27] In $[Ru_3(CO)_{10}SH]^-$, the Ru(1)–Ru(2) bond is supported by strong Ru(1)–S and Ru(2)–S bonds; the interaction of MO 63 of the fragment $[Ru_3(CO)_{10}]^{2-}$ with the tangential orbital of SH^+ gives rise to efficient ruthenium–sulfur σ-bonds (Figure 3b). The Mulliken overlap of +0.151 electron per bond is hardly perturbed at all when the bridging H^+ is introduced; while the metal–metal overlap falls drastically by 80%, the Ru–S overlap in fact increases by 6% (Table V). Thus, the metal–main-group atom bonding is playing a vital role in holding the two metal atoms together. This "clamp" effect is something of which experimental transition-metal cluster chemists are well aware. For example, Vahrenkamp[28] has

(27) Kostic, N. M.; Fenske, R. F. *Inorg. Chem.* **1983**, *22*, 666.
(28) Vahrenkamp, H. In "*Transition Metal Chemistry*; Müller, A., Diemann, E., Eds. Verlag Chemie: Basel, 1981; pp 35–60; *Adv. Organomet. Chem.* **1983**, *22*, 169.

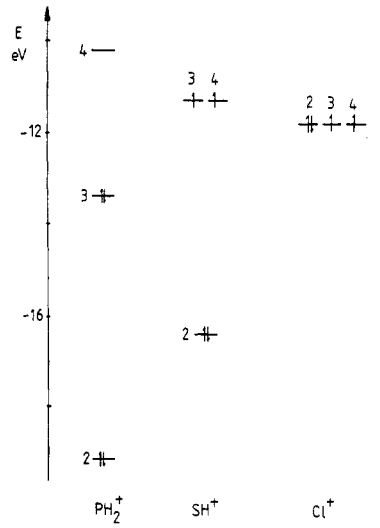

Figure 4. An energy level diagram to show the relative energies of the frontier MO's of the fragments PH_2^+, SH^+, and Cl^+. The energies are relative to those of the $[Ru_3(CO)_{10}]^{2-}$ fragment and are taken from the respective Fock matrices[23] of the complexes $HRu_3(CO)_{10}X$.

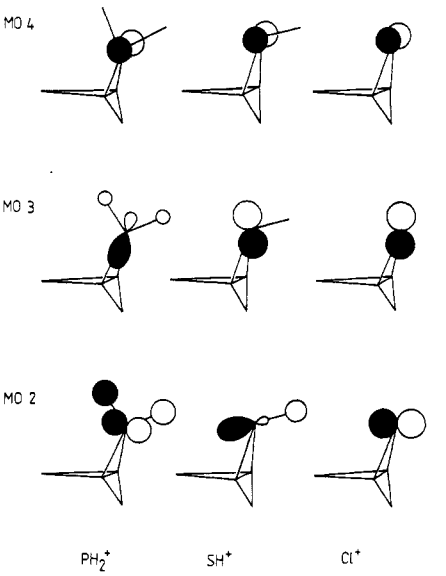

Figure 5. A schematic comparison of the frontier orbitals (MO's 2–4) of the bridgehead groups X (X = PH_2^+, SH^+, Cl^+) in the complex $HRu_3(CO)_{10}X$.

reviewed the ways in which cluster building reactions make use of metal–main-group atom bonds to stabilize M_xX units during cluster expansion. It has also been illustrated that the presence of a main-group cap or bridge in a transition-metal cluster can stabilize the cluster with respect to fragmentation during its reactions with Lewis bases.[29]

Comparisons within the Series $[HRu_3(CO)_{10}X]$ (X = PH_2, SH, Cl). The relative importance of the direct main-group ligand to metal (i.e. X–Ru) bonding and indirect (i.e. via the bridging moiety) Ru–Ru bonding in affecting the bridged Ru–Ru bond is assessed below. A periodic trend is covered by the model ligands, X, chosen. Table V illustrates the dependence on X of the Ru(1)–Ru(2), $Ru–X_{bridgehead-atom}$, and Ru–H bond overlap populations.

The bonding capabilities of X^+ are affected by the successive addition of hydrogen atoms to the group X that, inevitably, cause a rehybridization of the atomic orbitals at the bridgehead atom. Figure 4 compares the energy levels of the frontier orbitals of PH_2^+, SH^+, and Cl^+. Schematic representations of these MO's are shown in Figure 5. Obviously, in the case of Cl^+, the available frontier orbitals constitute a degenerate set of 3p orbitals. Moving from Cl^+ to SH^+ essentially protonates one 3p orbital, and going from SH^+ to PH_2^+ protonates a second. This gives rise to the splitting of the degeneracy shown in Figure 4. The important consequences of this rehybridization are as follows. First, the tangential orbital (MO 4) remains unperturbed in terms of symmetry but is lowered in energy in going from PH_2^+ through to Cl^+, i.e. the expected trend as the electronegativity of the bridgehead atom increases. This results in the energy of the tangential MO becoming less compatible with that of MO 63, the orbital of the $[Ru_3(CO)_{10}]^{2-}$ fragment with which it interacts. Hence, the MO in the final complex that results from the interaction of fragment MO's 63 and 4 contains a greater percentage of ligand character and a smaller percentage of metal character as one goes from a group 15 to a group 17 ligand. Thus, more electron density resides on the ligand rather than on the metal framework. Since MO

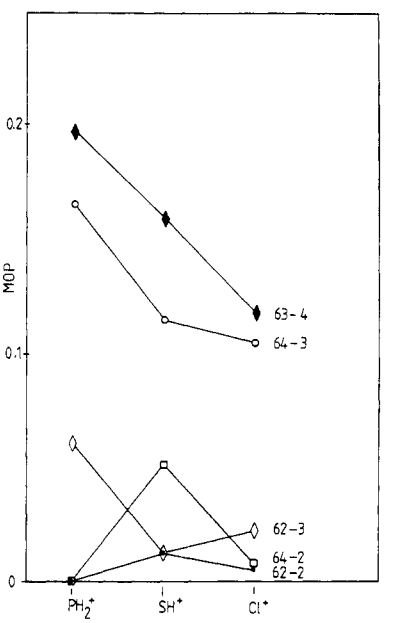

Figure 6. Plot of the interfragment Mulliken overlap populations (MOP) in $HRu_3(CO)_{10}X$ as a function of X (X = PH_2^+, SH^+, Cl^+) for the interactions between the frontier orbitals of $[Ru_3(CO)_{10}]^{2-}$ (MO's 62–64) and $[X]^+$ (MO's 2–4).

63 is Ru(1)–Ru(2) antibonding, this will lead to metal–metal bond strengthening along the series PH_2^+ to Cl^+.

Second, rehybridization of the orbitals at the bridgehead atom directly affects the nature of MO's 2 and 3 of X^+. Figure 5 illustrates that MO 3 for each ligand is derived from a radial p orbital. In both Cl^+ and SH^+, MO 3 has pure p character and varies only in its vectorial property. In PH_2^+, however, besides a reorientation of the p orbital component, MO 3 picks up 18% phosphorus 3s character. The enhanced directionality of this orbital is apparent if one compares the Mulliken overlap population of the LUMO (MO 64) of the $[Ru_3(CO)_{10}]^{2-}$ fragment with MO 3 for each X^+ fragment. This is shown graphically in Figure 6. The fall in overlap population from +0.164 in PH_2^+ to a value that shows little variation between SH^+ and Cl^+ is certainly a consequence of a change in hybridization and is not a function of a change in orbital energy (inspection of Figure 4 shows that, on energy grounds

(29) Housecroft, C. E.; Fehlner, T. P. *J. Am. Chem. Soc.* **1986**, *108*, 4867 and references therein.

alone, MO 3 in PH_2^+ is the *least* favorably disposed for interaction with metal fragment MO 64). The interaction of MO 3 of X^+ with MO 62 of $[Ru_3(CO)_{10}]^{2-}$ is relatively unimportant for SH^+ and Cl^+. However, the reorientation and hybridization of this radial orbital in PH_2^+ renders it suitable for good overlap with MO 62. Once again, the trend in Mulliken overlap populations for the 62–3 interaction (Figure 6) is not a function of orbital energy.

Despite the fact that interfragment interactions involving MO 2 are not as significant as those involving MO's 3 and 4, their variation in overlap populations as a function of X^+ is noteworthy. In Cl^+ and PH_2^+, the orbital properties of MO 2 are similar; the 29% contribution from each hydrogen atom occurring in PH_2^+ (Figure 5) does not affect the orbital symmetry with respect to cluster bonding. Both frontier orbitals give either zero or negligible overlap with the metal fragment orbitals 62 and 64. The zero vs finite 62–2 or 64–2 overlap in comparing MO 2 for PH_2^+ with Cl^+ is undoubtedly a result of the difference in energy of the two orbitals. However, for SH^+, MO 2 exhibits an sp hybrid that interacts quite effectively with the metal framework; the 64–2 interaction in $HRu_3(CO)_{10}SH$ shows a significant peak in the graph shown in Figure 6, while the 62–2 interaction shows a lesser one.

In the light of the above discussion, we suggest that in $HRu_3(CO)_{10}X$, for each bridge group X, an interaction involving a tangential p orbital on X is important in binding X to the metal framework. In the cases of X being SH and PH_2, hybridization at the bridgehead atom facilitates further interfragment interactions that bolster the metal to main-group atom bonding. Thus we are able rationalize the increase in Mulliken overlap that is observed for the direct $Ru–X_{bridgehead\text{-}atom}$ bonds in the order Ru–Cl < Ru–S < Ru–P (Table V).

Now let us consider how the Ru(1)–Ru(2) bonding is affected by the presence of different bridging groups, X, in $HRu_3(CO)_{10}X$. The following trends emerge from the data in Table IV. First, and most important, as one makes the periodic crossing from group 15 to 17, the increased loss of electron density from MO 63 of the $[Ru_3(CO)_{10}]^{2-}$ fragment is reflected in a gain in Ru(1)–Ru(2) overlap population since MO 63 is Ru(1)–Ru(2) antibonding. In going from X = PH_2 to SH to Cl, the trends in the final occupancies of metal fragment MO's 62 and 64 are less revealing than those of MO 63. The amount of charge transferred to MO 64 decreases marginally across the series, and consequently the resultant strengthening that the Ru(1)–Ru(2) bond experiences becomes slightly less. At the same time, the loss of electron density from MO 62, and hence the associated weakening of the metal–metal bond, remains approximately constant across the series. It is difficult to assess the net bond weakening caused by these two phenomena since one refers to a metal–metal σ-bond and one to a π-symmetry interaction (Figures 1 and 3). However, since the trend shown in Table V is one of *increasing* metal–metal overlap and is in accordance with the trend in observed bond lengths shown in Table I, we suggest that perhaps the interactions involving MO 63 of the $[Ru_3(CO)_{10}]^{2-}$ fragment predominate.

Our conclusion, then, is that in compounds of the type $HM_3(CO)_{10}X$, for the second-row main-group bridgehead atoms, metal–main-group atom bonding (considered as *indirect* metal–metal bonding) is responsible for the initial shortening of the bridged metal–metal bond. Along a periodic series, however, the bonding is finely tuned by *direct* metal–metal overlap. It is this fine tuning that results in the chloro ligand producing a greater shortening than the sulfido ligand which, in turn, produces greater shortening than the phosphido ligand in the characterized triosmium series. Structural characterization of the compound $HRu_3(CO)_{10}Cl$ has not, to date, been reported; we would predict that the bridged Ru–Ru bond distance will be shorter than 2.843 Å (Table I).

Acknowledgment. We gratefully acknowledge the SERC for a grant (S.M.O.) and the Royal Society for a 1983 Research Fellowship (C.E.H.). The Cambridge Crystallographic Data Base is also acknowledged for making available to us structural data. Dr. P. R. Raithby is thanked for helpful discussions.

Registry No. $HRu_3(CO)_{10}PH_2$, 114157-06-1; $HRu_3(CO)_{10}SH$, 114157-07-2; $HRu_3(CO)_{10}Cl$, 80800-55-1.